

# Ring Current Effects: Factors Affecting the NMR Chemical Shift of Molecules Adsorbed on Porous Carbons

*Alexander C. Forse,<sup>a</sup> John M. Griffin,<sup>a</sup> Volker Presser,<sup>b</sup> Yury Gogotsi,<sup>c</sup> Clare P. Grey<sup>\*a,d</sup>*

<sup>a</sup>Department of Chemistry, University of Cambridge, Lensfield Road, Cambridge CB2 1EW, UK

<sup>b</sup>INM – Leibniz Institute for New Materials & Saarland University, Campus D2 2, 66123

Saarbrücken, Germany

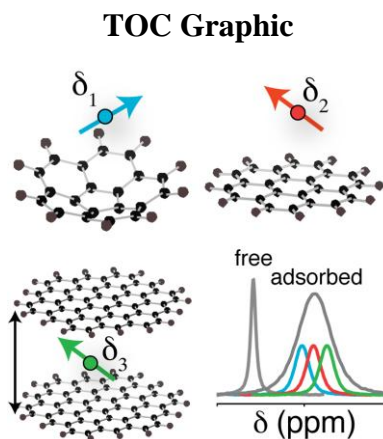
<sup>c</sup>Department of Materials Science and Engineering and A.J. Drexel Nanotechnology Institute, Drexel University, Philadelphia, PA 19104, USA

<sup>d</sup>Department of Chemistry, Stony Brook University, Stony Brook, New York, NY 11794-3400, USA

\*Corresponding author. Email: [cpg27@cam.ac.uk](mailto:cpg27@cam.ac.uk)

Nuclear magnetic resonance (NMR) spectroscopy is increasingly being used to study the adsorption of molecules in porous carbons, a process which underpins applications ranging from electrochemical energy storage to water purification. Here we present ab-initio calculations of the nucleus-independent chemical shift (NICS) near various  $sp^2$  hybridized carbon fragments to explore the structural factors that may affect the resonance frequencies observed for adsorbed species. The domain size of the delocalized electron system affects the calculated NICSs, with larger domains giving rise to larger chemical shieldings. In slit-pores, overlap of the ring current effects from the pore walls is shown to increase the chemical shielding. Finally, curvature in the carbon sheets is shown to have a significant effect on the NICS. The trends observed are consistent with existing NMR results

as well as new spectra presented for an electrolyte adsorbed on carbide-derived carbons prepared at different temperatures.



**Keywords** Nuclear Magnetic Resonance Activated Carbon Supercapacitor DFT Calculations

Porous carbons are used in a wide range of applications including the storage of charge in supercapacitors, gas storage, deionization of water, and purification of gases.<sup>1-4</sup> In each case the excellent adsorptive properties of the carbon are exploited to store molecules or ions. Porous carbons are typically prepared by the carbonization and subsequent chemical activation of organic matter such as coconut shells or wood.<sup>5</sup> The resulting amorphous carbon structure consists predominantly of hexagonal carbon rings in which the carbon is  $sp^2$ -hybridized.<sup>6</sup> They exhibit a combination of micropores (< 2 nm width), mesopores (2 – 50 nm) and macropores (> 50 nm), and offer extremely high surface areas for molecular adsorption (up to 3000  $m^2/g$ ). Porous carbons may also be prepared from inorganic precursors such as metal carbides. In this case, extraction of the metal atoms leaves a porous carbide-derived carbon (CDC) with a pore size that depends on the synthesis conditions.<sup>7-9</sup> Both methods allow the synthesis of carbons with porosity in the nanometer and sub-nanometer range, with CDCs well known for their narrow pore size distributions that can provide very high adsorption capacities for small gas molecules or electrolyte ions.<sup>10-12</sup>

Nuclear magnetic resonance (NMR) spectroscopy has proven to be a particularly useful technique for studying molecular adsorption inside microporous carbon. When the nuclear spins in the adsorbate are studied, separate resonances are observed for adsorbed and free species.<sup>13–24</sup> Regardless of the nuclear spin studied, resonances arising from adsorbed molecules are shifted to lower frequencies relative to their free counterparts. This is because the species close to carbon surfaces experience a locally reduced magnetic field owing to the circulation of nearby delocalized  $\pi$  electrons in the carbon. As such, to a first approximation such ‘ring-current’ effects are nucleus-independent.<sup>25</sup> However, if the carbon adsorbent is varied, differences in chemical shielding are observed for a given adsorbate, implying that different carbon structures give rise to different ring-current effects.<sup>15,18</sup>

For a known carbon structure, first-principles calculations can be performed to determine isotropic chemical shielding values ( $\sigma_{\text{iso}}$ ) at arbitrary positions above and around the structure.<sup>26</sup> The isotropic nucleus-independent chemical shift at that position,  $\delta_{\text{iso}}^{\text{NICS}}$  (referred to more generally as the NICS here) is then given by  $-(\sigma_{\text{iso}} - \sigma_{\text{ref}})$ , where  $\sigma_{\text{ref}}$  is zero in this case. The NICS is a measure of the change in chemical shift that may be expected due to the influence of the carbon ring-currents. Such calculations have been performed on idealized carbon systems such as graphene sheets, nanotubes and fullerenes.<sup>27–30</sup> However, amorphous carbons exhibit more complicated structures thought to consist of curved graphene-like sheets and fullerene-like elements arranged in a highly disordered fashion.<sup>6,31–33</sup> As such, calculations on the basic carbon building blocks offer a convenient starting point to determine structural properties. For example, Moran *et al.* performed NICS calculations on a series of polybenzenoid hydrocarbons of increasing cluster size, though they did not consider distances from the carbon relevant to molecular adsorption.<sup>34</sup> We recently calculated NICSs on a small graphene-like carbon fragment to interpret the resonance frequencies of electrolyte ions adsorbed in the micropores of an activated carbon supercapacitor electrode.<sup>24</sup> The validity of using finite molecular units to model structural and magnetic properties of bulk graphene has also recently been demonstrated.<sup>35</sup>

In this work, NICS calculations are performed on a series of model carbon fragments to explore the structural factors that affect the resonance frequencies of adsorbed species. First, the effect of the size of graphene-like domains is considered, and is shown to have significant effects on the local magnetic field. We then show that the width of model carbon slit-pores has a considerable effect on the chemical shielding inside the pores due to overlap of the shielding effects from each pore wall. Experimental NMR data is then presented for an electrolyte adsorbed on a series of carbide-derived carbons prepared at different temperatures. Carbons prepared at higher temperatures are shown to bring about a greater chemical shielding for adsorbed ions. This is rationalized by considering the sizes of the graphene-like domains in the carbons and the predictions made by the NMR calculations.

Ab-initio structure optimisations and NMR calculations were performed in Gaussian 03 software,<sup>36</sup> at the B3LYP level of theory with the 6-31G(d) basis set. Previous work showed that NICSs calculated near aromatic hydrocarbons do not vary significantly when different basis sets are used.<sup>37</sup> Positions less than 3 Å away from the carbon planes were not considered as it is unlikely that molecules will be able to probe these distances due to the Van der Waals radii of the carbon and the probe molecule.<sup>38</sup> Figure 1a shows NICS values calculated at different heights ( $z$ ) above the ring plane of coronene, with three different positions in the  $x$ - $y$  plane being considered. For all positions studied, negative NICS values were calculated. The results show that the NMR resonance from a nucleus in a molecule adsorbed above coronene should appear at a lower frequency (to the right hand side of the spectrum) than the resonance from the free molecule. This result is in qualitative agreement with experimental data that consistently reveals shielding effects for species adsorbed in porous carbons.<sup>15,18,24</sup>

The calculated shielding is greatest for small distances above the centre of coronene, and at large distances the NICS tends towards zero (Figure 1a). Moreover, as positions more remote from the coronene centre (in the  $x$ - $y$  plane) are considered (see position A to B to C) the magnitudes of the NICSs tend to decrease. For example, the calculated value at 3 Å above the centre of the external 6-

membered ring (position C, an ‘edge’ site) is -3.6 ppm, compared to -4.4 ppm at 3 Å above the central ring (position A).

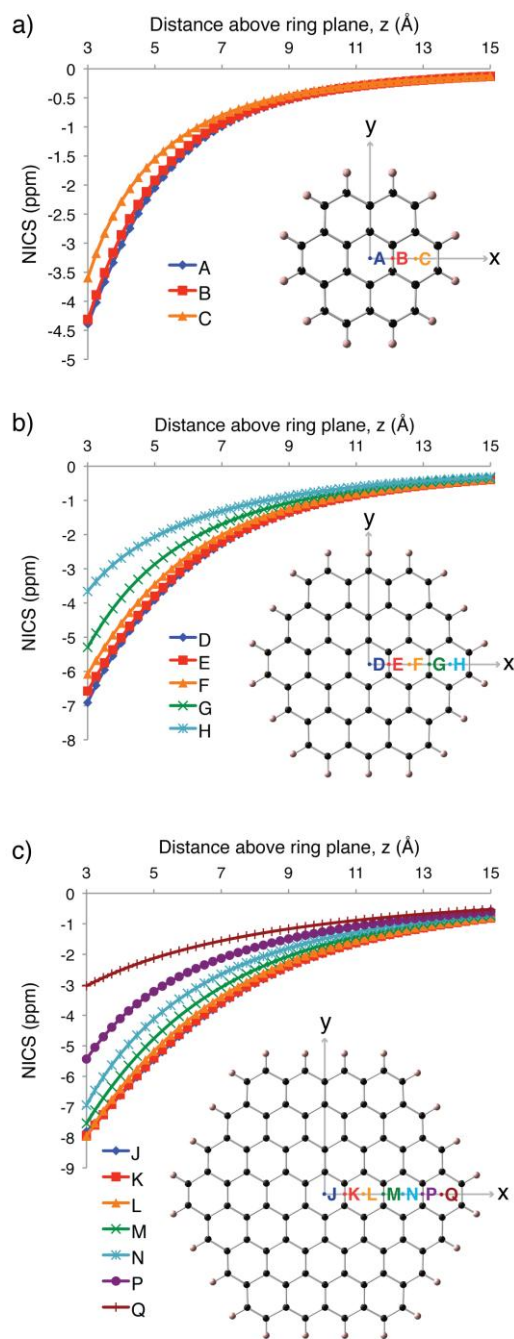


Figure 1: NICS calculations on a) coronene, b) circumcoronene and c) dicircumcoronene. Insets show the optimized structures as well as positions in x-y where values were calculated.

For carbons derived from both organic and inorganic precursors, the size of the graphene-like domains tends to increase for higher synthesis temperatures.<sup>8,39,40</sup> To explore the effect of the graphene domain size on the NICS, further calculations were performed on a series of coronene-based

molecules of larger size. Calculated NICSs for circumcoronene and dicircumcoronene (Figure 1b and c) show similar trends to coronene, with the largest shielding effects calculated above the ring centres. Importantly, the NICSs above the molecular centres are found to increase with the molecular size. This trend is in agreement with previous NICS calculations used to interpret intermolecular shielding effects in the solid state structures of aromatic molecules.<sup>37,41</sup> Here, the maximum calculated NICS varies from -4.4 to -6.9 to -7.8 ppm as the coronene diameter is increased from 7.5 Å to 12.4 Å to 17.3 Å, respectively. These calculations suggest that a porous carbon with more ordered hexagonal bonding and larger graphene-like domains should bring about greater shielding effects for adsorbate molecules. More disordered carbons with smaller graphene-like domains and more edge sites will result in smaller shielding effects. In real porous carbon particles, a liquid or gaseous adsorbate will experience a range of carbon structures during the NMR timescale at ambient temperatures. Indeed, 2D NMR exchange experiments have shown that electrolyte ions undergo chemical exchange in and out of the carbon micropores on a millisecond timescale.<sup>19,22,23</sup> As such, experimentally observed chemical shifts will arise from a dynamic averaging of chemical shifts associated with many different adsorption sites.

In a porous carbon, molecules may experience the ring-current effects from multiple carbon surfaces within the carbon pores. To probe the effect of well-defined carbon pore sizes on the chemical shifts of adsorbates, NICS calculations were performed on model slit-pores consisting of two individually optimized circumcoronene (C<sub>54</sub>H<sub>18</sub>) molecules (sheets) separated by a distance, *d* (see Figure 2a). In each case, NICSs were calculated at positions within the pore along the *z*-axis, which coincides with the C<sub>6</sub> symmetry axis, and positions less than 3 Å from the carbon sheets were not considered.

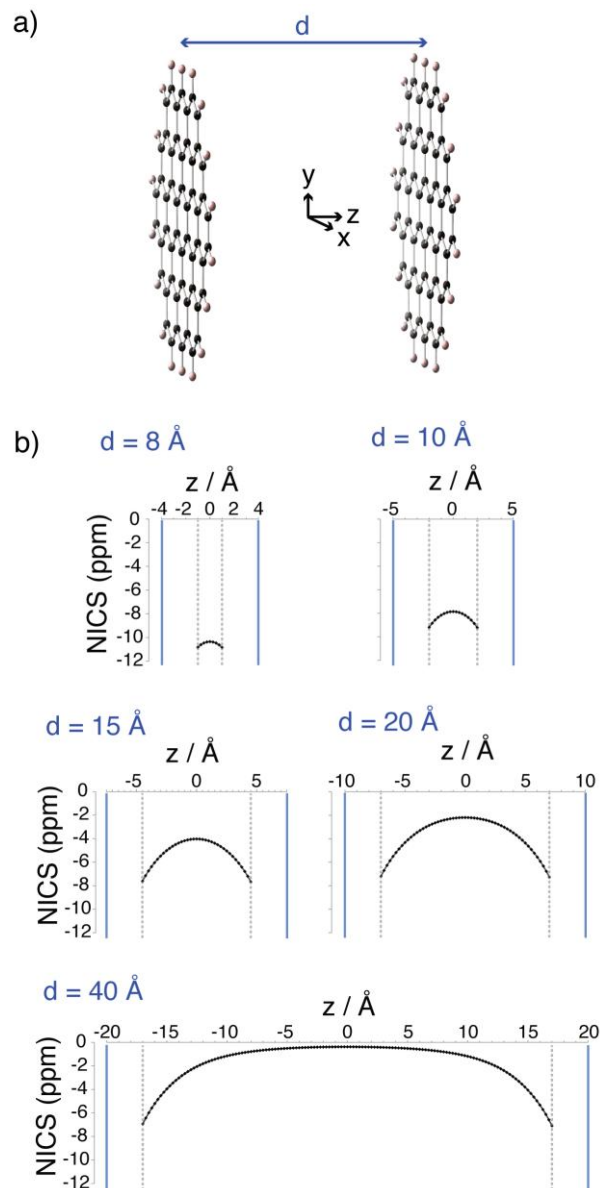


Figure 2: a) geometry of model slit pores comprising two circumcoronene molecules. b) NICS calculations for slit pores with different sizes. Blue solid lines represent the positions of the pore walls. NICS values were calculated between the dotted grey lines.

NICSs are shown in Figure 2b for a range of different pore widths, with negative NICSs calculated for all positions considered. This shows that the NMR resonance from a nucleus in a molecule within a carbon pore should again appear at a lower frequency than the resonance from the free molecule. For small pores (e.g.  $d = 8$  Å), considerable overlap of the shielding effects from the pore walls brings about large NICS values with only small variations across the pore. As the pore size is increased, this overlap becomes less significant and for a large pore (e.g.  $d = 40$  Å) the overlap is negligible.

Importantly, as the pore size is decreased, larger absolute NICS values are calculated. Comparison of the NICS values calculated for the slit-pores with values calculated above a single circumcoronene molecule (Figure 1b) show that the effects of the two circumcoronenes (i.e. the pore walls) are additive to a very good approximation (see Supporting Information). Knowing this, NICS values may readily be generated for a range of different pore sizes given the knowledge of NICS values for a given carbon fragment.

Again, the effects of dynamics must be considered as fast exchange between different adsorption sites will result in an averaging of the observed chemical shift. Indeed, a single NMR resonance was observed experimentally for species adsorbed in a porous carbon with a bimodal pore size distribution, showing that there is fast exchange within the porous network.<sup>22</sup> As such it is very reasonable to expect fast exchange between the different positions within a pore. Averaging of the NICSs calculated here yields values of -10.6, -8.3, -5.2, -3.7, and -1.7 ppm for slit (circumcoronene) pores of width 8, 10, 15, 20, and 40 Å, respectively. While it may be more appropriate to perform a weighted average taking into account the effect of the adsorption thermodynamics, the general trend of greater chemical shielding with decreasing pore size will remain unchanged. This qualitative trend agrees well with recent experimental work by Borchardt *et al.*,<sup>22</sup> where magic angle spinning (MAS) <sup>11</sup>B NMR spectra of the electrolyte NEt<sub>4</sub>BF<sub>4</sub> in acetonitrile (1 M) on a series of carbons with well-controlled pore sizes showed that as the average pore size is decreased the chemical shielding experienced by ions in the pores increases. <sup>1</sup>H NMR studies of hydrogen gas adsorbed on a series of activated carbons revealed a similar trend, though in this case carbons with a broader pore size distribution were studied.<sup>18,42</sup> Quantitative comparison of the calculated NICSs with experimental values should be avoided, as the model slit-pores we have considered do not capture the complicated disordered structures of real porous carbons.

Previous work has indicated that the ordered domain size of porous CDC increases with synthesis temperature.<sup>33,40</sup> To probe the effect of carbon synthesis temperature on the resonance frequency of



adsorbed ions, MAS NMR experiments were performed on a series of titanium carbide-derived carbons (TiC-CDCs) soaked with the electrolyte  $\text{NEt}_4\text{BF}_4$  in acetonitrile (1.5 M). TiC-CDCs prepared via chlorine gas treatment at 600, 800 and 1000 °C, denoted TiC-CDC-600, -800 and -1000, respectively, were studied and Figure 3 shows the  $^{19}\text{F}$  MAS NMR spectra (see Supporting Information and Ref. 21 for more details on the experimental procedure). For each carbon soaked with electrolyte, two peaks are observed for  $\text{BF}_4^-$  as in our previous work.<sup>21</sup> Ex-pore resonances arise from anions between primary particles in the carbon film, with a very similar resonance frequency to the neat electrolyte. The in-pore resonances arise from anions adsorbed inside the carbon micropores, shielded by the carbon ring currents. Across the series, the in-pore resonance becomes more shielded, the difference between the in-pore and neat electrolyte chemical shifts varying from -2.6 to -4.0 to -5.4 ppm for TiC-CDC-600, -800 and -1000, respectively. This is despite slight increases in the average pore size (see Supporting Information) of 8.15, 9.06 and 9.32 Å, respectively, which are expected to bring about the opposite effect. The same trend is observed in  $^1\text{H}$  NMR spectra (this time probing the  $\text{NEt}_4^+$  cations) recorded on the same samples (see Supporting Information), showing that the effect is nucleus-independent. We also note that for TiC-CDCs synthesized at higher temperatures, the line width of the in-pore resonance increases. This is tentatively ascribed to a combination of the broader pore size distributions (see Supporting Information) and increased electronic conductivities<sup>40</sup> of TiC-CDCs prepared at higher temperatures.

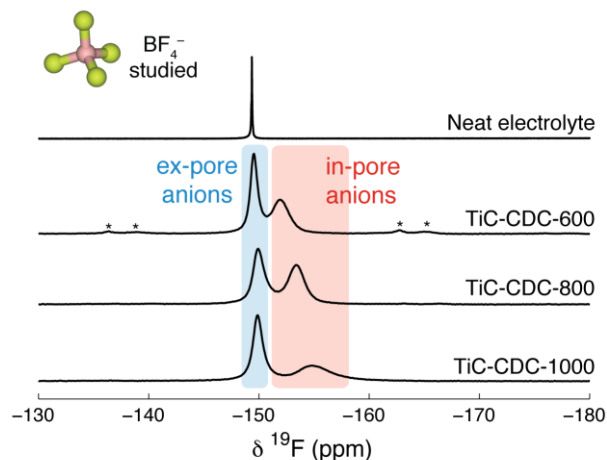


Figure 3:  $^{19}\text{F}$  MAS (5 kHz) NMR of different TiC-CDCs soaked with  $\text{NEt}_4\text{BF}_4$  in acetonitrile electrolyte. Asterisks mark spinning sidebands.

The results agree with recent work where  $^{11}\text{B}$  MAS NMR showed that resonances from in-pore  $\text{BF}_4$  anions in TiC-CDC-1000 were more shielded than those in TiC-CDC-600.<sup>22</sup> This was rationalized by noting that TiC-CDC-600, with a lower synthesis temperature, is a more disordered carbon with more  $\text{sp}^3$ -hybridized carbon. In our case, however, we note that  $^{13}\text{C}$  NMR experiments on isotopic  $\text{Ti}^{13}\text{C}$ -CDC do not show any peaks indicative of  $\text{sp}^3$ -hybridized carbon, but instead contain only a single broad resonance at  $\sim 125$  ppm due to  $\text{sp}^2$ -hybridized carbon (see Supporting Information). Raman spectroscopy (see Supporting Information), magnetic susceptibility measurements,<sup>40</sup> and structural simulations using molecular dynamics<sup>33</sup> show that as the temperature used in the synthesis is increased, the carbon structure becomes more ordered on a local scale with larger graphene-like domains. The calculations presented in Figure 1 then help explain the variation of chemical shift observed for in-pore (adsorbed) ions in carbide-derived carbons: for the case of TiC-CDC, the effect of structural carbon ordering dominates any pore-size effects.

It has been suggested that non-hexagonal rings in the carbon sheets of porous carbons brings about their curved amorphous structures.<sup>6,31</sup> Indeed, 5-membered rings have recently been detected by transmission electron microscopy of an activated carbon.<sup>43</sup> As such, molecular species adsorbed

inside porous carbons may experience a range of different curved carbon structures, as well as planar ones.<sup>44</sup>

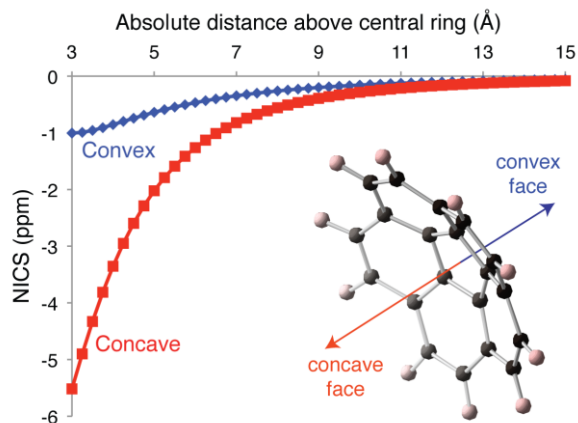


Figure 4: NICS calculations on corannulene.

To probe the effect of curvature on the NICS, calculations were performed on corannulene, which represents a fragment of a fullerene molecule and has a characteristic bowl shape (see inset, Figure 4). NICSs were calculated along the  $C_5$  symmetry axis on both the convex and concave faces of corannulene (Figure 4). On both faces negative NICSs were calculated, though the magnitude of the NICSs are considerably greater on the concave face. While a maximum NICS of -1.0 ppm is calculated on the convex face (at 3 Å from the central ring plane), the maximum NICS on the concave face is -5.5 ppm. The corresponding value for planar coronene is -4.4 ppm (Figure 1a), intermediate between the maximum values calculated for the two faces of corannulene. This suggests that porous carbons exhibiting different amounts of concave, convex and planar surfaces will bring about different chemical shifts for adsorbed molecules, though the effect of dynamic averaging should again be considered. Deschamps *et al.* recently observed two different NMR environments for adsorbed ions inside activated carbons.<sup>23</sup> In addition to resonances arising from ‘type I’ ions adsorbed between graphene-like sheets, a less shielded resonance arising from ‘type II’ adsorption sites was observed and was postulated to arise from ions near 5- or 7-membered carbon rings. Given the results presented here, it is possible that such a type II resonance arises from ions inside regions of the carbon exhibiting a relatively large number of convex carbon surfaces. However, based on the calculations in

Figure 1, type II resonances may also arise from ions inside regions of the carbon with more edge sites.

In conclusion, ab-initio calculations have been used to explore the different structural factors affecting the resonance frequencies observed for species adsorbed in porous carbons. In particular we conclude:

1. Larger graphene-like domains result in greater chemical shielding at distances relevant to molecular adsorption.
2. Smaller carbon slit-pores result in greater chemical shieldings due to overlap of the ring-current effects from each pore wall. These results agree qualitatively with recent experimental data.
3. TiC-CDCs prepared at higher temperatures are shown to bring about a greater chemical shielding for adsorbed ions. This is ascribed to an increase in the structural ordering of the carbon with larger graphene-like domains.
4. Curvature of the carbon surfaces has a marked effect on the NICSs, with convex surfaces bringing about greater chemical shielding than concave surfaces.

We envisage that the observation of these trends will aid the future interpretation of experimental NMR data for molecules adsorbed on porous carbons. Going further, this work offers the possibility of characterizing porous carbons on the basis of the chemical shifts of adsorbed molecules.

### **Supporting Information**

Details of NICS calculations, experimental details, discussion of additivity of NICSs from pore walls, pore size distributions,  $^{13}\text{C}$  NMR and Raman spectra of TiC-CDCs and  $^1\text{H}$  NMR spectra of TiC-CDCs soaked with electrolyte. This material is available free of charge via the Internet at <http://pubs.acs.org>

### **Notes**

The authors declare no competing financial interests.

## Acknowledgments

ACF, JMG, and CPG acknowledge the Sims Scholarship (ACF), EPSRC (via the Supergen consortium; JMG) and the EU ERC (via an Advanced Fellowship to CPG) for funding. CDC synthesis at Drexel University was supported by the U.S. Department of Energy, Office of Science, Basic Energy Sciences, under Award #ER46473. VP acknowledges funding from the German Federal Ministry for Research and Education (BMBF) in support of the nanoEES3D project (award number 03EK3013) as part of the strategic funding initiative energy storage framework and thanks Prof. Eduard Arzt (INM) for his continuing support. Mohamed Shamma and Boris Dyatkin (Drexel University) are thanked for their support in the synthesis of CDC material. Ab-initio calculations were performed using the Darwin Supercomputer of the University of Cambridge High Performance Computing Service (<http://www.hpc.cam.ac.uk/>), provided by Dell Inc. using Strategic Research Infrastructure Funding from the Higher Education Funding Council for England and funding from the Science and Technology Facilities Council. Finally, we thank Hao Wang, Patrice Simon, Phoebe Allan, Nicole Trease, Andy Ilott, Céline Merlet, Beth Howe and Tim Dickens for useful discussions.

## References

- (1) Simon, P.; Gogotsi, Y. Capacitive Energy Storage in Nanostructured Carbon-Electrolyte Systems. *Acc. Chem. Res.* **2013**, *46*, 1094–1103.
- (2) Porada, S.; Zhao, R.; van der Wal, A.; Presser, V.; Biesheuvel, P. M. Review on the Science and Technology of Water Desalination by Capacitive Deionization. *Prog. Mater. Sci.* **2013**, *58*, 1388–1442.
- (3) Ismail, A. F.; David, L. I. B. A Review on the Latest Development of Carbon Membranes for Gas Separation. *J. Membr. Sci.* **2001**, *193*, 1–18.
- (4) Candelaria, S. L.; Shao, Y.; Zhou, W.; Li, X.; Xiao, J.; Zhang, J.-G.; Wang, Y.; Liu, J.; Li, J.; Cao, G. Nanostructured Carbon for Energy Storage and Conversion. *Nano Energy* **2012**, *1*, 195–220.
- (5) Marsh, H.; Rodriguez-Reinoso, F. Activated Carbon. *1st ed.*; Elsevier Science Ltd. **2006**.

- (6) Harris, P. New Perspectives on the Structure of Graphitic Carbons. *Crit. Rev. Solid State Mater. Sci.* **2005**, *30*, 235–253.
- (7) Gogotsi, Y.; Nikitin, A.; Ye, H.; Zhou, W.; Fischer, J. E.; Yi, B.; Foley, H. C.; Barsoum, M. W. Nanoporous Carbide-derived Carbon with Tunable Pore Size. *Nat. Mater.* **2003**, *2*, 591–594.
- (8) Dash, R.; Chmiola, J.; Yushin, G.; Gogotsi, Y.; Laudisio, G.; Singer, J.; Fischer, J.; Kucheyev, S. Titanium Carbide Derived Nanoporous Carbon for Energy-related Applications. *Carbon* **2006**, *44*, 2489–2497.
- (9) Presser, V.; Heon, M.; Gogotsi, Y. Carbide-Derived Carbons - From Porous Networks to Nanotubes and Graphene. *Adv. Funct. Mater.* **2011**, *21*, 810–833.
- (10) Sevilla, M.; Mokaya, R. Energy Storage Applications of Activated Carbons: Supercapacitors and Hydrogen Storage. *Energy Environ. Sci.* **2014**, in press, DOI: 10.1039/C3EE43525C.
- (11) Chmiola, J.; Yushin, G.; Gogotsi, Y.; Portet, C.; Simon, P.; Taberna, P.-L. Anomalous Increase in Carbon Capacitance at Pore Sizes Less Than 1 Nanometer. *Science* **2006**, *313*, 1760–1763.
- (12) Borchardt, L.; Oschatz, M.; Kaskel, S. Tailoring Porosity in Carbon Materials for Supercapacitor Applications. *Mater. Horiz.* **2014**, in press: DOI: 10.1039/c3mh00112a.
- (13) Harris, R. K.; Thompson, T. V.; Norman, P. R.; Pottage, C.; Trethewey, A. N. High-resolution  $^2\text{H}$  Solid-state NMR of  $2\text{H}_2\text{O}$  Adsorbed onto Activated Carbon. *J. Chem. Soc., Faraday Trans.* **1995**, *91*, 1795–1799.
- (14) Harris, R. K.; Thompson, T. V.; Norman, P. R.; Pottage, C. Adsorption Competition onto Activated Carbon, Studied by Magic-angle Spinning NMR. *J. Chem. Soc. Faraday. Trans.* **1996**, *92*, 2615–2618.
- (15) Harris, R. K.; Thompson, T. V.; Norman, P. R.; Pottage, C. Phosphorus-31 NMR Studies of Adsorption onto Activated Carbon. *Carbon* **1999**, *37*, 1425–1430.

- (16) Dickinson, L. M.; Harris, R. K.; Shaw, J. A.; Chinn, M.; Norman, P. R. Oxygen-17 and Deuterium NMR Investigation into the Adsorption of Water on Activated Carbon. *Magn. Reson. Chem.* **2000**, *38*, 918–924.
- (17) Lee, S.-I.; Saito, K.; Kanehashi, K.; Hatakeyama, M.; Mitani, S.; Yoon, S.-H.; Korai, Y.; Mochida, I. <sup>11</sup>B NMR Study of the Anion in Activated Carbons at Various Stages of Charge of EDLCs in Organic Electrolyte. *Carbon* **2006**, *44*, 2578–2586.
- (18) Anderson, R. J.; McNicholas, T. P.; Kleinhammes, A.; Wang, A.; Liu, J.; Wu, Y. NMR Methods for Characterizing the Pore Structures and Hydrogen Storage Properties of Microporous Carbons. *J. Am. Chem. Soc.* **2010**, *132*, 8618–8626.
- (19) Wang, H.; Köster, T. K.-J.; Trease, N. M.; Ségalini, J.; Taberna, P.-L.; Simon, P.; Gogotsi, Y.; Grey, C. P. Real-time NMR Studies of Electrochemical Double-layer Capacitors. *J. Am. Chem. Soc.* **2011**, *133*, 19270–19273.
- (20) Liu, X.; Pan, X.; Shen, W.; Ren, P.; Han, X.; Bao, X. NMR Study of Preferential Endohedral Adsorption of Methanol in Multiwalled Carbon Nanotubes. *J. Phys. Chem. C* **2012**, *116*, 7803–7809.
- (21) Forse, A. C.; Griffin, J. M.; Wang, H.; Trease, N. M.; Presser, V.; Gogotsi, Y.; Simon, P.; Grey, C. P. Nuclear Magnetic Resonance Study of Ion Adsorption on Microporous Carbide-derived Carbon. *Phys. Chem. Chem. Phys.* **2013**, *15*, 7722–7730.
- (22) Borchardt, L.; Oschatz, M.; Paasch, S.; Kaskel, S.; Brunner, E. Interaction of Electrolyte Molecules with Carbon Materials of Well-defined Porosity: Characterization by Solid-state NMR Spectroscopy. *Phys. Chem. Chem. Phys.* **2013**, *15*, 15177–15184.
- (23) Deschamps, M.; Gilbert, E.; Azais, P.; Raymundo-Piñero, E.; Ammar, M. R.; Simon, P.; Massiot, D.; Béguin, F. Exploring Electrolyte Organization in Supercapacitor Electrodes with Solid-state NMR. *Nat. Mater.* **2013**, *12*, 351–358.

- (24) Wang, H.; Forse, A. C.; Griffin, J. M.; Trease, N. M.; Trognko, L.; Taberna, P.-L.; Simon, P.; Grey, C. P. In Situ NMR Spectroscopy of Supercapacitors: Insight into the Charge Storage Mechanism. *J. Am. Chem. Soc.* **2013**, *135*, 18968–18980.
- (25) Lazzeretti, P. Ring Currents. *Prog. in Nucl. Magn. Reson. Spectrosc.* **2000**, *36*, 1–88.
- (26) Chen, Z.; Wannere, C. S.; Corminboeuf, C.; Puchta, R.; Schleyer, P. v. R. Nucleus-independent Chemical Shifts (NICS) as an Aromaticity Criterion. *Chem. Rev.* **2005**, *105*, 3842–3888.
- (27) Sebastiani, D. Current Densities and Nucleus-Independent Chemical Shift Maps from Reciprocal-Space Density Functional Perturbation Theory Calculations. *Chem. Phys. Chem.* **2006**, *7*, 164–175.
- (28) Kibalchenko, M.; Payne, M. C.; Yates, J. R. Magnetic Response of Single-walled Carbon Nanotubes Induced by an External Magnetic Field. *ACS Nano* **2011**, *5*, 537–545.
- (29) Ren, P.; Zheng, A.; Pan, X.; Han, X.; Bao, X. DFT Study on the NMR Chemical Shifts of Molecules Confined in Carbon Nanotubes. *J. Phys. Chem. C* **2013**, *117*, 23418–23424.
- (30) Bühl, M. The Relation Between Endohedral Chemical Shifts and Local Aromaticities in Fullerenes. *Chem. Eur. J.* **1998**, *4*, 734–739.
- (31) Harris, P. J. F. Fullerene-like Models for Microporous Carbon. *J. Mater. Sci.* **2013**, *48*, 565–577.
- (32) Harris, P. J. F. Structure of Non-graphitising Carbons. *Int. Mater. Rev.* **1997**, *42*, 206–218.
- (33) Palmer, J. C.; Llobet, A.; Yeon, S.-H.; Fischer, J. E.; Shi, Y.; Gogotsi, Y.; Gubbins, K. E. Modeling the Structural Evolution of Carbide-derived Carbons Using Quenched Molecular Dynamics. *Carbon* **2010**, *48*, 1116–1123.
- (34) Moran, D.; Stahl, F.; Bettinger, H. F.; Scafer III, H. F.; Schleyer, P. v. R. Towards Graphite : Magnetic Properties of Large Polybenzenoid Hydrocarbons. *J. Am. Chem. Soc.* **2003**, *125*, 6746–6752.



- (35) Vähäkangas, J.; Ikäläinen, S.; Lantto, P.; Vaara, J. Nuclear Magnetic Resonance Predictions for Graphenes: Concentric Finite Models and Extrapolation to Large Systems. *Phys. Chem. Chem. Phys.* **2013**, *15*, 4634–4641.
- (36) M. J. Frisch, G. W. Trucks, H. B. Schlegel, G. E. S.; M. A. Robb, J. R. Cheeseman, J. A. Montgomery, Jr., T. V.; K. N. Kudin, J. C. Burant, J. M. Millam, S. S. Iyengar, J. T.; V. Barone, B. Mennucci, M. Cossi, G. Scalmani, N. R.; G. A. Petersson, H. Nakatsuji, M. Hada, M. Ehara, K. T.; R. Fukuda, J. Hasegawa, M. Ishida, T. Nakajima, Y. Honda, O. K.; H. Nakai, M. Klene, X. Li, J. E. Knox, H. P. Hratchian, J. B. C.; V. Bakken, C. Adamo, J. Jaramillo, R. Gomperts, R. E. S.; O. Yazyev, A. J. Austin, R. Cammi, C. Pomelli, J. W. O.; P. Y. Ayala, K. Morokuma, G. A. Voth, P. Salvador, J. J. D.; et al. Gaussian 03, Revision E.01.
- (37) Facelli, J. C. Intermolecular Shielding from Molecular Magnetic Susceptibility. A New View of Intermolecular Ring Current Effects. *Magn. Reson. Chem.* **2006**, *44*, 401–408.
- (38) Bondi, A. Van Der Waals Volumes and Radii. *J. Phys. Chem.* **1965**, *68*, 441–451.
- (39) Zickler, G. A.; Smarsly, B.; Gierlinger, N.; Peterlik, H.; Paris, O. A Reconsideration of the Relationship Between the Crystallite Size  $L_a$  of Carbons Determined by X-ray Diffraction and Raman Spectroscopy. *Carbon* **2006**, *44*, 3239–3246.
- (40) Vora, P.; Gopu, P.; Rosario-Canales, M.; Pérez, C.; Gogotsi, Y.; Santiago-Avilés, J.; Kikkawa, J. Correlating Magnetotransport and Diamagnetism of  $sp^2$ -bonded Carbon Networks through the Metal-insulator Transition. *Phys. Rev. B* **2011**, *84*, 1–8.
- (41) Ma, Z.; Halling, M. D.; Solum, M. S.; Harper, J. K.; Orendt, A. M.; Facelli, J. C.; Pugmire, R. J.; Grant, D. M.; Amick, A. W.; Scott, L. T. Ring Current Effects in Crystals. Evidence from  $^{13}C$  Chemical Shift Tensors for Intermolecular Shielding in 4,7-di-*t*-butylacenaphthene Versus 4,7-di-*t*-butylacenaphthylene. *J. Phys. Chem. A* **2007**, *111*, 2020–2027.

- (42) McNicholas, T. P.; Wang, A.; Neill, K. O.; Anderson, R. J.; Stadie, N. P.; Kleinhammes, A.; Parilla, P.; Simpson, L.; Ahn, C. C.; Wang, Y.; et al. H<sub>2</sub> Storage in Microporous Carbons from PEEK Precursors. *J. Phys. Chem. C* **2010**, *114*, 13902–13908.
- (43) Harris, P. J. F.; Liu, Z.; Suenaga, K. Imaging the Atomic Structure of Activated Carbon. *J. Phys.: Condens. Matter* **2008**, *20*, 362201.
- (44) Merlet, C.; Péan, C.; Rotenberg, B.; Madden, P. A.; Daffos, B.; Taberna, P.-L.; Simon, P.; Salanne, M. Highly Confined Ions Store Charge More Efficiently in Supercapacitors. *Nat. Comm.* **2013**, *4*, 2701.